Linkoping Studies in Science and Technology
Licentiate Thesis No. 1520

The Effect of Mg Doping on Optical and Structural Properties of GaN

Sergey Khromov

Linköping University
INSTITUTE OF TECHNOLOGY

LIU-TEK-LIC-2012:5
Thin Film Physics Division
Department of Physics, Chemistry and Biology (IFM)
Linkoping University
SE-581 83 Linkoping, Sweden

ISBN: 978-91-7519-950-4
ISSN 0280-7971
Printed by LiU-Tryck
Linköping, Sweden, 2012

Abstract

Mg is the most commonly used *p*-type dopant for GaN, however the impact of Mg incorporation on structural, morphological and optical properties of GaN is still not fully understood. Another research challenge is to understand and improve the properties of nonpolar GaN as it allows the fabrication of more efficient optoelectronic devices due to the absence of polarization fields.

Thus, the aim of this thesis was to explore the effect of Mg doping on polar *c*-plane GaN in **Paper 1** and nonpolar *m*-plane GaN in **Paper 2**. The samples were grown by metal-organic vapor phase epitaxy with varying Mg content on free-standing GaN substrates. The studies were done by transmission electron microscopy (TEM) and low temperature cathodoluminescence (CL) with the aim to correlate the optical and structural data obtained by these techniques.

Polar *c*-plane GaN:Mg layers exhibit such structural defects as stacking faults (SF) of a small size (5-10 nm). The basal plane SF (BSF) density was estimated to be $\sim 10^5 - 10^6$ cm^{-1} increasing with Mg concentrations. Comparison between as-grown and annealed samples has not shown significant difference in structural or optical properties. Characteristic broad emission lines observed in CL in the range of $3.29 - 3.41$ eV have been attributed to SF-related emissions by analogy with nonpolar undoped GaN films grown heteroepitaxially. Acceptor bound exciton (ABE) emission and SF-related peaks have demonstrated metastability. CL mapping performed on the TEM samples at the energies corresponding to SF-related peaks has confirmed that the origin of these lines is associated with Mg-doped GaN layers. In nonpolar *m*-plane GaN:Mg layers similar BSFs have been

observed. In addition more extended BSFs and prismatic SFs were identified at the interface with the GaN substrate. For the m-plane samples with Mg concentration of $\sim 10^{19}$ cm^{-3} a number of fine CL lines have been detected in the region of 3.3-3.4 eV. Their shape and appearance were unlike the SF-related emissions in the case of c-plane GaN discussed in **Paper 1**. These peaks are not likely to be associated with donor-acceptor pair (DAP) recombination as has been proved by estimation of the separated DAP energies and by CL mapping experiment. A tentative explanation is given to these peaks as being related to excitons bound to some low symmetry acceptor defect centers.

Preface

This Licentiate Thesis is a result of two and a half years' work during my Ph. D. studies in Thin Film Physics group at Linköping University. The project was financed by Swedish Energy Agency and the Swedish Research Council (VR). The results are presented in two included papers preceded by the introduction.

Linköping, February 2012

Included Papers

Paper 1 **Luminescence related to high density of Mg-induced stacking faults in homoepitaxially grown GaN**
S. Khromov, C. G. Hemmingsson, H. Amano, B. Monemar, L. Hultman, and G. Pozina
Physical Review B 84, 075324 (2011)

Paper 2 **Optical and structural studies of homoepitaxially grown m-plane GaN**
S. Khromov, B. Monemar, V. Avrutin, Xing Li, H. Morkoç, L.Hultman, and G. Pozina
Submitted for publication

Papers not included in the Thesis

Paper 3 **Growth of GaN nanotubes by halide vapor phase epitaxy**
C. Hemmingsson, G. Pozina, **S. Khromov** and B. Monemar
Nanotechnology 22 (2011) 085602

Paper 4 **Effect of silicon and oxygen doping on donor bound excitons in bulk GaN**
G. Pozina, **S. Khromov**, C. Hemmingsson, L. Hultman, and B. Monemar
Physical Review B 84, 165213 (2011)

Acknowledgements

I would like to express my gratitude to the people who supported me and helped me in writing of this Thesis. Special thanks goes to:

- Galia Pozina, my supervisor
- Lars Hultman, my co-supervisor
- Co-authors
- Colleagues at Thin Film, Plasma and Nanostructured Materials groups
- My family and friends

Contents

Chapter 1

Introduction

Since the invention of light emitting diode (LED) technology and demonstration of the laser diode (LD) in 1960s there began a search for materials that would be suitable to make efficient optoelectronic devices based on these effects. Soon it was understood that II-VI and III-V group materials are appropriate for this task. III-V semiconductor GaAs and its compounds were used in manufacturing of high efficiency red to yellow LEDs and LDs. To produce high brightness full-color displays or to make high brightness white sources of light an efficient blue LED was, however, needed. Possible candidates for short-wavelength LEDs were II-VI material ZnSe and indirect bandgap semiconductor SiC, but short lifetimes of ZnSe-based devices and low efficiencies of SiC-based LEDs severely limited their use [1]. GaN, on the other hand, looked much more promising for production of short wavelength devices.

The research on GaN started in the early 1970s when it was realized that GaN and its compounds with Al and In is a suitable material system to cover the green to violet wavelength region for light emitters (Fig. 1.1). GaN is a III-V group semiconductor with a relatively large direct bandgap energy of 3.4 eV. GaN crystallizes in wurtzite or cubic structures, however, the last one is metastable. Due to its high vapor pressure of 45000 atm. and high melting point temperature of 2500^{o}C it is almost impossible to grow single crystals of GaN from liquid phase. Therefore methods that employ growth from vapor phase are used, such as molecular-beam epitaxy (MBE), halide vapor phase epitaxy (HVPE) or metal-organic vapor phase epitaxy (MOCVD). The first violet LED

based on GaN was demonstrated by Maruska and Pankove in 1972, however, the further development of GaN-based devices was hindered in 1970s and 1980s by low crystalline quality and p-type doping issues.

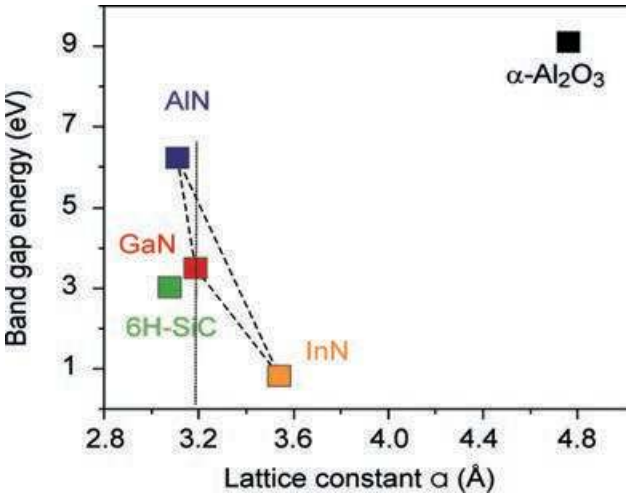

Figure 1.1: Bandgap energies of III-V nitrides as a function of their lattice constants.

The introduction of a low-temperature buffer layer of AlN on sapphire substrates at the initial growth stages by Amano and Akasaki in 1986 [2] led to a considerable improvement of crystal quality of epitaxial GaN. Later in 1989 the same group solved the p-type doping problem. Magnesium was known to be a good p-type dopant, nevertheless it was difficult to obtain sufficient hole concentration due to passivation of Mg atoms by hydrogen, which comes from precursors during the MOCVD growth. Amano and Akasaki proposed low energy electron irradiation as a means to activate the charge carriers thus increasing hole concentration to suitable values of 10^6 cm^{-3} [3]. Later thermal annealing in N_2 ambient was also suggested to activate the Mg acceptors [4]. As a result of such development Nakamura demonstrated in 1993 the first bright blue and green GaN heterostructure-based LEDs with more than 100 times higher efficiency compared to other alternatives [5].

This breakthrough brought about ever increasing research efforts towards

more efficient and brighter blue and white LEDs based on GaN and eventually to a revolution in lighting that we are witnessing right now. Besides solid-state lighting GaN-based devices find applications in full-color LED displays and indicators, data storage (Blu-ray technology uses GaN-based LDs), telecommunications (optical fiber networks), high power electronics and many others.

One of the remaining challenges on the way to produce better devices is the lack of native substrates for GaN, therefore growth on sapphire (α-Al_2O_3) or silicon carbide (6H-SiC) is usually done for commercial purposes. Growth on foreign substrates leads to a high dislocation density due to a substantial difference in lattice constants (Fig. 1.1) and in thermal expansion coefficients. Threading dislocation density in GaN grown on sapphire is $\sim 10^8 - 10^9$ cm^{-2} [6] and it is surprising that working devices exist with such a high density of defects. Threading dislocations serve as nonradiative recombination centers [7] and as scattering centers that affect carrier mobility [8], [9]. Other extended defects include stacking faults (SFs) and associated with them partial dislocations. They are typical for non-polar grown GaN where the density of SFs and partial dislocations is typically 10^5 cm^{-1} and 10^{10} cm^{-2}, respectively [10]. In conventional polar GaN layers Mg can be a factor facilitating formation of such SFs as it was observed in **Paper 1**. These defects can play a role of the additional localization potential for carriers and show characteristic emissions in the region of 3.29-3.41 eV [11].

The structural defects have detrimental effect on optoelectronic devices because they increase the current threshold in emitters, cause leakage in the form of dark current in detectors and lower working lifetimes. Therefore, better understanding of extended defects in GaN as well as effect of Mg doping on crystalline quality is needed. The aim of this thesis is the study of structural defects and their influence on optical properties in epitaxial films of Mg-doped GaN grown by metal-organic chemical vapor deposition.

Chapter 2

Growth Techniques

When heated at atmospheric pressure GaN dissociates rather than melts, thus growth from liquid solution at reasonable conditions is impossible as it mentioned above. Therefore vapor phase deposition techniques are used for GaN synthesis; three major methods exist nowadays, MBE, HVPE and MOCVD, which will be described in more detail.

2.1 Molecular Beam Epitaxy

MBE is a non-equilibrium vapor phase epitaxy growth method where solid or gas source elements are heated in evaporators, known as Knudsen effusion cells, to produce beams of atoms impinging on the substrate, which is rotated and heated to appropriate temperatures. The effused atoms need to have mean free paths bigger than the size of the chamber, also to obtain films of sufficient purity low levels of residual gases must be sustained, therefore ultra-high vacuum (10^{-9} Torr) is needed, which is the drawback of this method. The advantages are the lower, compared to other methods, growth temperatures of $600 - 800^{o}$C and possibility to grow very thin layers with fine control of composition. Precision of this growth technique is based on low deposition rates and in-situ characterization capabilities. For example, reflection high energy electron diffraction (RHEED) detector allows to control the thickness of the film up to one atomic monolayer.

Conventional Knudsen cells are used as sources of Ga and possible dopant

elements, such as Si for n-type and Mg for p-type. On the other hand, plasma nitrogen sources are normally employed for nitrogen source. The two nitrogen atoms in the N_2 molecule are connected with three covalent bonds that results in a very high cohesive energy. Therefore, it is easier to dissociate N_2 molecule in a plasma environment. Radio frequency (RF) plasma sources are used and the modified method for growth of III-nitrides is called plasma assisted MBE (PAMBE). Nevertheless this method remains more of a research tool due to quite low growth rates (typically < 1 μm/h [12]) and rather sophisticated equipment.

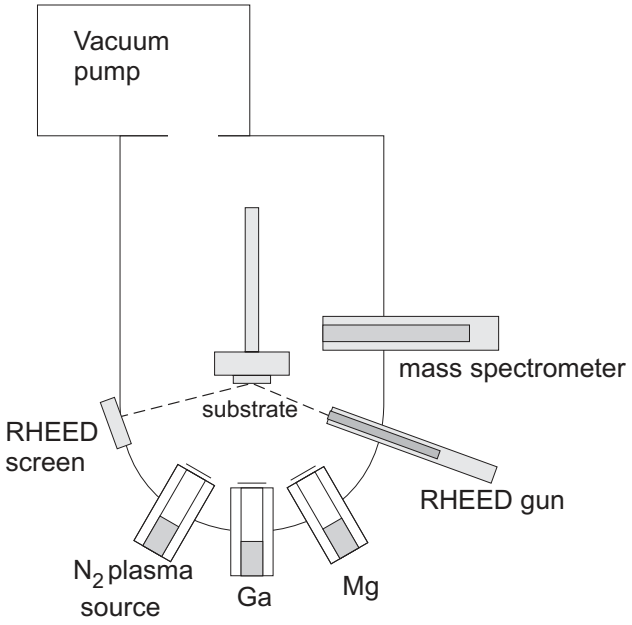

Figure 2.1: Schematic drawing of MBE chamber for GaN growth.

2.2 Halide Vapor Phase Epitaxy

A typical horizontal hot wall HVPE reactor is depicted on Fig. 2.2. The chamber is made of quartz and can be heated resistively or by RF induction. There are

two temperature zones. The metallic source zone is kept at the temperature of $\sim 800-900^{o}$C, which is lower than the growth zone temperature ($1000-1100^{o}$C). By using several temperature zones more flexibility in controlling and in adjusting growth conditions can be achieved.

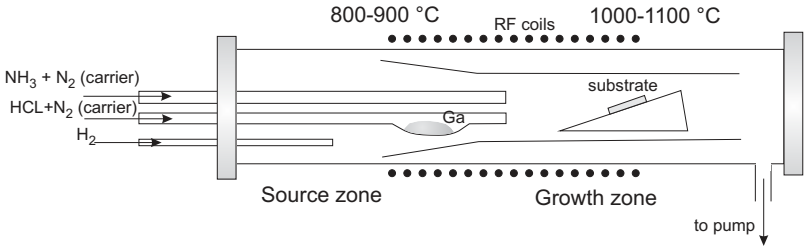

Figure 2.2: Schematic drawing of HVPE growth reactor.

Hydrogen chloride is let into the quartz tube with melt Ga where the reaction producing gallium chloride occurs:

$$2\mathrm{Ga} + 2\mathrm{HCl} \rightarrow 2\mathrm{GaCl} + \mathrm{H_2}$$

The efficiency of this process is very high, above 95% [13]. In a separate tube NH_3, the group V source, is flowed. Subsequently ammonia and gallium chloride undergo the following reaction on the surface of the substrate:

$$\mathrm{GaCl} + \mathrm{NH_3} \rightarrow \mathrm{GaN} + \mathrm{HCl} + \mathrm{H_2}$$

To prevent parasitic growth in the gas inlet ammonia and halide (GaCl) should not be mixed before they reach the substrate. Light molecule gases such as H_2 or mixtures of N_2 and H_2 are used as carrier gases to obtain laminar flow. The deposition rate is $\sim 100-300$ μm/h and is very high compared to MBE, which is why HVPE is commercially used for growing thick GaN layers. The process occurs at atmospheric pressure, at near equilibrium conditions and is mass transport limited by the flow of halide precursor. The 300-μm-thick freestanding GaN substrates for the samples in **Paper 1** were grown by HVPE.

2.3 Metal-organic Chemical Vapor Deposition

MOCVD is a technique similar to HVPE, only instead of inorganic species metal-organic precursors are flown in the reactor as sources of Ga. Specifically trimethylgallium ($(CH_3)_3Ga$) is used as Ga, and ammonia – as nitrogen precursors. For Mg doping organic compounds are used too, for instance for samples in **Paper 1** bis-cyclopentadienylmagnesium (Cp_2Mg) was employed. Alternatively silane (SiH_4) can be used as a source for Si (n-type) doping of GaN. Organic species and ammonia are transported in separate pipes to the quartz chamber to prevent premature reacting. Lighter carrier gases (H_2 or N_2) are let through organic compound liquids thus transporting the precursors to the reactor. These compounds are thermally dissociated over the surface of $\sim 1000^oC$ hot substrate and react in a sequence of complex reactions forming GaN. In hot wall MOCVD the whole reactor is heated by RF coils, whereas in the cold-wall process only the susceptor, which is usually made of graphite, is heated. The substrate may be rotated to obtain uniform films. Before the growth is started nitridation of the substrate is usually done to reduce lattice mismatch due to the nitrides formed on the substrate surface (SiN on SiC or AlN on Al_2O_3). The usual practice is to start epitaxial growth on sapphire substrates with a low-temperature ($\sim 600^oC$) GaN buffer layer. Ease of scalability, high uniformity and quality of the films, and a relatively high growth rates (~ 1 μm/h) are making this technique the method of choice for commercial purposes. Undoped $0.5 - \mu m$-thick buffer layer and 1-μm-thick Mg-doped epitaxial layer for samples in **Paper 1** were grown by MOCVD. In **Paper 2** 400 nm Mg-doped layer, starting with an undoped 0.6 μm GaN, were grown by this method as well.

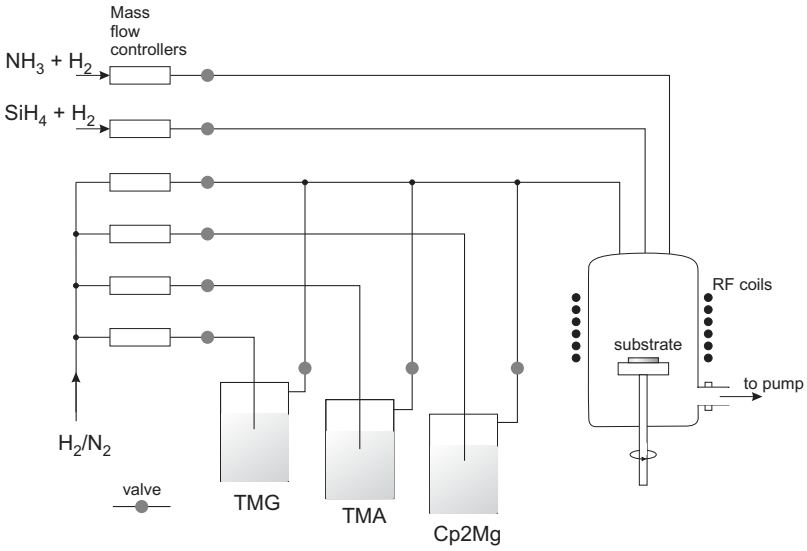

Figure 2.3: Schematic drawing of hot wall MOCVD reactor that can be used for growth of GaN and/or AlN. TMG stands for trimethylgallium, TMA – for trimethylalluminium and Cp2Mg – for bis-cyclopentadienylmagnesium.

Chapter 3

Properties of GaN

As all other III-nitrides GaN has partially covalent and partially ionic bonds. The GaN iconicity is relatively high that explains the significant hardness and chemical stability of GaN. Other superior material properties such as high electron mobility, high thermal conductivity, and high critical field combined with direct wide bandgap make GaN attractive for many electronic and optoelectronic applications.

3.1 Crystallographic Properties

GaN has two polytypes: zinc blende, also known as sphalerite (space group $F\bar{4}3m$ and wurtzite (space group $P6_3mc$), the former being cubic and the latter being hexagonal structure. Cubic form of GaN is only metastable so most of the research is focused on wurtzite GaN. The wurtzite structure can be imagined as two interpenetrating hexagonal closed packed (hcp) lattices, consisting of the corresponding element atoms, shifted by 3/8 of the cell height, Fig. 3.1.

Each Ga atom is surrounded by four N atoms and vice versa, i.e. atoms are tetrahedrally coordinated in GaN. The basis (highlighted, Fig. 3.1) consists of four atoms, two of each type, their coordinates are the following: Ga atom (0, 0, 0), $(\frac{1}{3}, \frac{2}{3}, \frac{1}{2})$ and N atom (0, 0, u), $(\frac{1}{3}, \frac{2}{3}, \frac{1}{2} + u)$. There are two different positions for atoms in the wurtzite structure and the stacking sequence can be written as AaBbAa, where capital letters denote Ga atoms and small ones – N atoms. It is

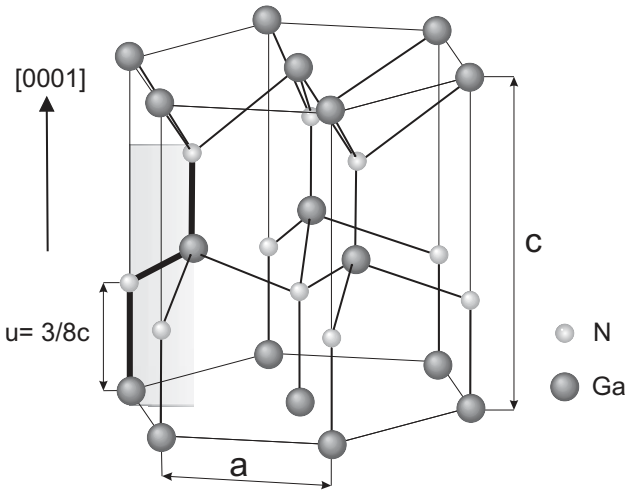

Figure 3.1: Unit cell of wurtzite GaN. The four basis atoms are highlighted.

interesting to compare stacking sequences of zinc blende and wurtzite structures, Fig. 3.2, because it can help understand how SFs are formed for example. Zinc blende structure, in difference to wurtzite, consists of three alternating bilayers of atoms: AaBbCc.

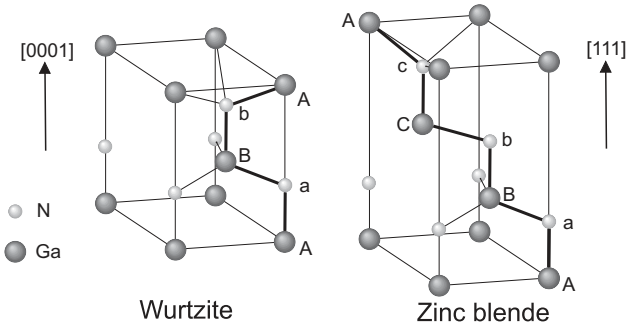

Figure 3.2: Stacking sequences of wurtzite and zinc blende GaN.

3.2 Polarity and Polarization

Wurtzite GaN is a non-centrosymmetric crystal, which means that the directions [0001] and [000$\bar{1}$] are not equivalent. Thus, there are two orientations: the Ga- and N-faces with Ga and N atoms in the top position of the bilayer, respectively (Fig. 3.3). It is important to mention that Ga-face does not mean that the surface is terminated by Ga atoms. For example, N-face surface can be terminated by Ga atoms. Thus, termination is a property of the surface, but not the growth orientation, which is fixed by the orientation of the first grown bilayer.

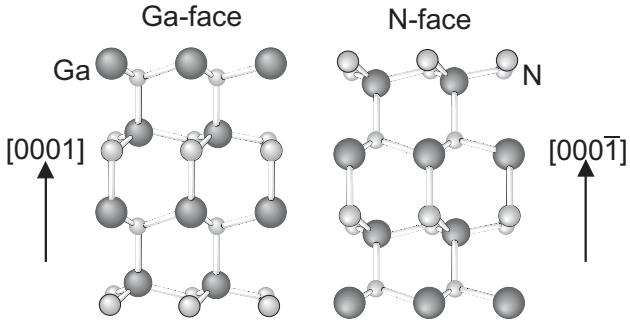

Figure 3.3: The two different orientations of GaN.

Polarity of the film defines surface properties and direction of spontaneous polarization in the crystal [14]. Spontaneous polarization is an intrinsic property of the material and "related to the deviation of the crystal lattice parameters from the ideal values for the structure, thereby creating molecular dipoles in the material building up a macroscopic polarization field much like in the ferroelectrics" [15]. Besides spontaneous polarization, piezoelectric field is present in the film due to the stress generated by growth on foreign substrates, and, additionally, by stress in heterostructures, therefore total polarization is the sum of the two components:

$$\vec{P}_{tot} = \vec{P}_{spon} + \vec{P}_{piezo}$$

Presently most of the GaN optoelectronic devices are based on *c*-direction grown films. These devices employ quantum wells (QWs) - heterostructures where thin

layers of narrower bandgap material are grown in the wider bandgap material matrix, for instance InGaN/GaN or AlGaN/GaN. QWs allow confinement of charge carriers and dramatically increase probability of their radiative recombination. On the other hand the built-in polarization field leads to bending of the bandgap therefore spatially separating the charge carriers (Fig. 3.4). This phenomena is

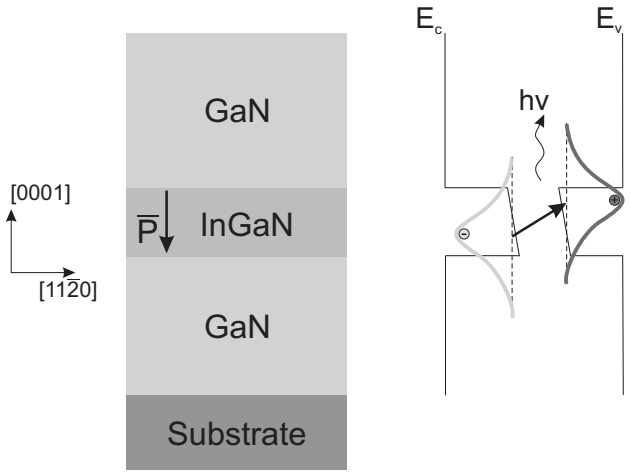

Figure 3.4: Energy band bending in InGaN/GaN QW structure.

called quantum confined Stark effect and is detrimental for optoelectronic devices as it lowers radiative recombination probability and thus quantum efficiency as well as red-shifting the output emission [15].

3.3 Nonpolar Growth Directions

To solve the problem of high polarization fields present in *c*-plane GaN, growth on nonpolar planes was initiated. There are two nonpolar sets of planes: *a*-planes, $\{11\bar{2}0\}$, and *m*-planes, $\{10\bar{1}0\}$, Fig. 3.5. The research on nonpolar GaN was hindered for a long time by technological problems in growing films with smooth morphologies on foreign substrates. A seminal paper was published by Waltereit et al. in 2000 [16] where nonpolar *m*-plane heterostructures of GaN/AlGaN grown

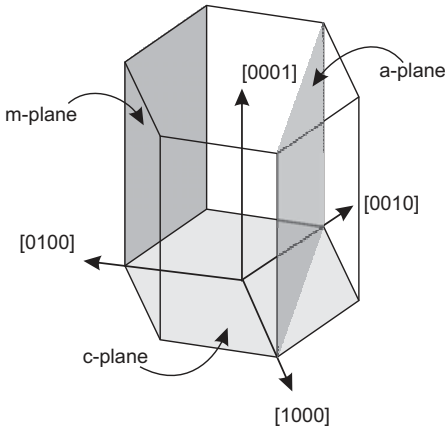

Figure 3.5: Polar (*c*-) and nonpolar (*m*- and *a*-) planes in GaN.

on tetragonal $LiAlO_2$ were reported. After this publication interest to nonpolar GaN was boosted and working devices based on m-plane GaN were produced recently [17], [18]. Higher concentration of extended defects compared to *c*-plane films, especially SFs, is the main problem of nonpolar GaN nowadays, and the question of the exact mechanism of their formation remains to be answered.

Chapter 4

Optical Transitions in GaN

When we intentionally excite electrons to the conduction band using optical or electrical pumping a number of optical transitions during recombination is possible in GaN, as illustrated in Fig. 4.1. Donor and acceptor levels are depicted

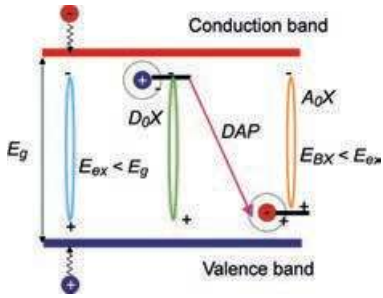

Figure 4.1: Main optical transitions in GaN.

by short lines inside the bandgap. A direct recombination of excess electron from the donor level with the hole bound to the acceptor level is possible and called donor-acceptor pair (DAP) recombination. Donor and acceptor atoms are neutral before and become charged after the recombination, therefore Coulomb interaction energy is added to the radiative recombination energy:

$$E(r) = E_g - (E_D + E_A) + \frac{e^2}{4\pi\epsilon_0\epsilon r}$$

Excitonic recombinations make up another important type of transitions. Exciton is an electrically neutral quasiparticle consisting of an electron and a hole bound by an electrostatic Coulomb force. Generally excitons are divided into two kinds: more tightly bound, the so-called Frenkel excitons, with typical binding energy in the range 0.1-1 eV and more weakly bound, Wannier-Mott (WM) excitons, with typical binding energy of $\sim 0.01 - 0.03$ eV. GaN possesses a reasonably high dielectric constant, $\epsilon = 8.9$, therefore electrostatic field in electron-hole pair is reduced and only weakly bound WM excitons with energies of ~ 25 meV are present. It can be noted that the exciton binding energy is described by a simple Bohr model of hydrogen atom:

$$E_{ex}(n) = -\frac{m_r e^4}{8\epsilon_0^2 \epsilon^2 h^2 n^n} = -\frac{13.6}{\epsilon^2 n^2}\left(\frac{m_r}{m_i}\right) \qquad (eV)$$

where $m_r = \frac{m_e^\star m_h^\star}{m_e^\star + m_h^\star}$ is the reduced electron-hole effective mass, h is Planck's constant, $m_e^\star$ and $m_h^\star$ are effective mass of electron and hole, respectively, and ϵ_0 is electric constant ($\approx 8.854 \times 10^{-12}$ F/m). When recombined, the WM exciton gives off energy in the following radiative form:

$$h\nu = E_g - E_{ex}$$

Excitons can form complexes with donor or acceptor impurity atoms (Fig. 4.2) and even structural defects [19]. Donor and acceptor bound emission are denoted by D_oX and A_oX in Fig. 4.1. When bound excitons recombine they emit the energy that can be expressed as follows:

$$h\nu = E_g - E_{ex} - E_{BX},$$

where E_{BX} is the binding energy of the exciton to the donor or acceptor atom. Bound excitons are important for characterization since they serve as optical signature of impurities.

GaN is a direct bandgap semiconductor with the energy dispersion curves around Γ point of reciprocal space schematically depicted in Fig. 4.3. The valence band top is split off into three subbands due to the crystal-field splitting and spin-

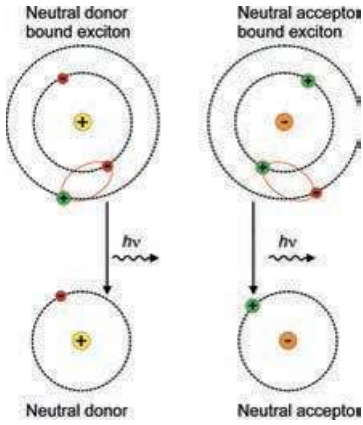

Figure 4.2: Schematic drawing of bound exciton electronic structure and the corresponding recombination process.

orbital coupling [20], consequently there are three excitons – A, B and C that involve a hole from each of the subbands. DAP, free exciton (FE), and bound

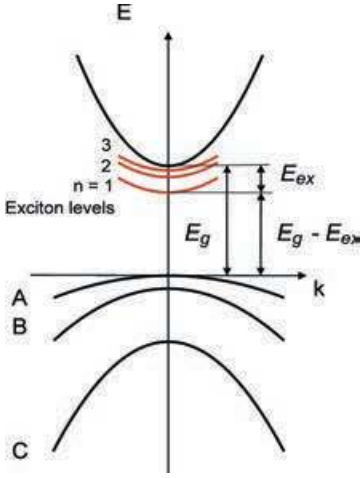

Figure 4.3: Schematic drawing of energy dispersion curves of GaN at Γ point of Brillouin zone.

exciton (BE) emissions are commonly called near bandgap emission (NBE). A typical spectrum of NBE from *c*-plane HVPE-grown GaN is shown in Fig. 4.4. Besides DAP (at the inset, larger scale), three FE lines, acceptor and donor BE we can see longitudinal optical (LO) phonon replicas of the same peaks in the 3.35-3.40 eV region. Intense exciton-longitudinal optical phonon interaction also takes place owing to high ionicity of bonds in GaN and according to the Frohlich polar intraband scattering theory [21]. LO phonon interaction induces phonon-assisted exciton emissions accompanying the exciton recombination. The ratio of the exciton peak intensities to the intensities of phonon replicas serves as a measure of exciton-phonon interaction.

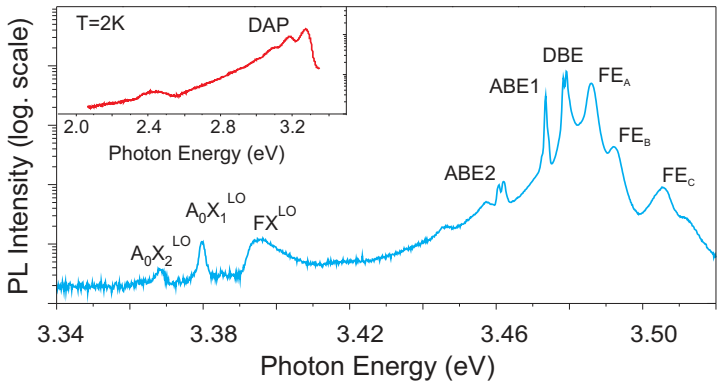

Figure 4.4: The photoluminescence spectrum of nominally undoped HVPE-grown GaN taken at 2 K. Courtesy of Dr. G. Pozina.

Chapter 5

Extended Defects in GaN

It was mentioned in introduction that low availability of cheap and high quality native substrates drives manufacturers to grow GaN on foreign substrates, such as SiC or sapphire. It results in high strain fields due to lattice mismatch and difference of temperature expansion coefficients between the epitaxial film and the substrate, which in turn leads to high density of extended defects, such as threading dislocations (TD) and SFs. Extended defects proved to have limited effect on device performance and working devices exist despite extremely high density of TDs in the range $10^8 - 10^9$ cm^{-2} [6] and SFs in the range $10^5 - 10^6$ cm^{-2} [22]. However, they do influence device performance, e.g., TDs can act as scattering centers thus lowering carrier mobility [23], and non-radiative recombination centers which lowers quantum efficiency [7]; SFs were linked with higher leakage currents [24]. Therefore, to produce new generations of LEDs, the density of extended defects must be lowered [25] and a lot of research is concentrated in this direction.

5.1 Threading Dislocations

There are normally three types of TDs in c-plane GaN (Fig. 5.1): perfect edge (a-type) dislocations with Burger vector $\mathbf{b} = \frac{1}{3}\langle 11\bar{2}0\rangle$ and line vector $\mathbf{J} = \langle 0001\rangle$, they constitute 40-70% of all dislocations [26]; perfect screw dislocations (c-type) with $\mathbf{b} = \langle 0001\rangle$ and $\mathbf{J} = \langle 0001\rangle$, they are the most uncommon type and are 1-2%

of all dislocations [23],[27]. The rest are mixed type dislocations ($a+c$-type) with $\mathbf{b} = \frac{1}{3}\langle 11\bar{2}3\rangle$ and l about 12^o inclined from the [0001] direction, [23].

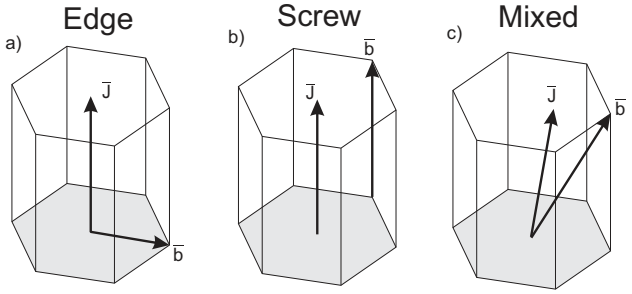

Figure 5.1: Dislocation types in GaN and their corresponding Burger vectors b and line directions J. a) Edge dislocation (a-type). b) Screw dislocation (c-type). c) Mixed dislocation ($a+c$-type).

There is controversy regarding the origin of TDs. Ning *et al*. [28] proposed that the rotation of the coalescence islands during the initial growth stages results in TD formation. They suggested that rotation of the islands around [0001] axis leads to their tilt and consequent formation of edge TDs while rotation around axes perpendicular to [0001] leads to their twist and screw TDs formation (Fig. 5.2). These findings were supported by Wu *et al*. [29]. On the other hand Narayanan *et al*. [30] in their studies stated that TDs come from the defects at the sapphire/GaN boundary.

.

Different methods are used to lower the TD density, such as epitaxial lateral overgrowth, pendeo epitaxy [31], applying high-temp AlN buffer layers [25] or transitional metal nitrides interlayers [32]. These techniques allowed to lower the dislocation density by several orders of magnitude to $\sim 10^6 - 10^7$ cm^{-2}.

In my studies I investigated homoepitaxially grown c-plane (**Paper 1**) and m-plane (**Paper 2**) GaN using TEM and we did not observe any disclocations in the films therefore we can conclude that the TD density was much lower than 10^6 cm^{-2} in our samples.

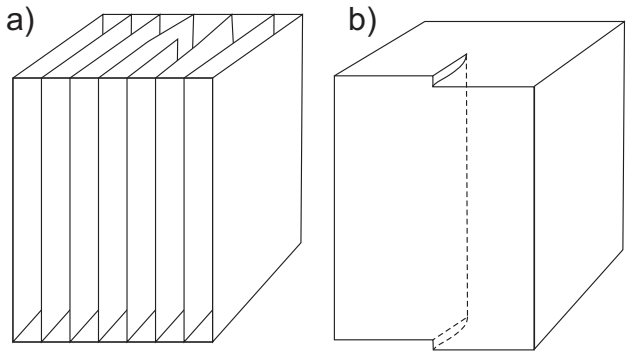

Figure 5.2: a) Perfect edge dislocation. b) Perfect screw dislocation.

5.2 Stacking Faults

SFs are normally observed in nonpolar GaN [11],[22], but can also be detected in *c*-plane GaN, **Paper 1**. Three kinds of BSFs are typical for GaN, two intrinsic ones – I_1 and I_2, and one extrinsic – E, Fig. 5.3.

Intrinsic BSF of type I_1 is formed by removing one layer (e.g., Aa) in hexagonal AaBbAaBb stacking followed by slip of the rest of the crystal by $\frac{1}{3}\langle 10\bar{1}0\rangle$ to reduce the fault energy. This type of SF is bound by Frank partial dislocation with Burger vector $\mathbf{b} = \frac{1}{6}\langle 2\bar{2}03\rangle$. I_2 SF is a result of direct shearing by $\langle 10\bar{1}0\rangle$ of one part of the crystal in respect to the other or, alternatively, by dissociation of a perfect dislocation into two Shockley partial dislocations with Burger vectors $\mathbf{b} = \frac{1}{3}\langle 1\bar{1}00\rangle$. Extrinsic SF is formed by insertion of an extra layer of atoms in the stacking and bound by Frank partials of type $\mathbf{b} = \frac{1}{2}[0001]$ [22].

SFs can be imagined as a thin lamella of zinc blende GaN introduced in the wurtzite lattice, each of them possessing a characteristic SF energy γ. The magnitude of γ depends on the number of violations in the stacking sequence of the planes [33]. I_1 SF involves one change, I_2 SF – two changes and E SF – three changes. Ratios of energies for different kinds of SFs can roughly be written as $\gamma_E \approx \frac{3}{2}\gamma_{I_2} \approx 3\gamma_{I_1}$. I_1 SF has the lowest energy and therefore should be the most probable type of SFs. This is supported by the experiments – I_1 is the most commonly observed SF, followed by I_2 and E types.

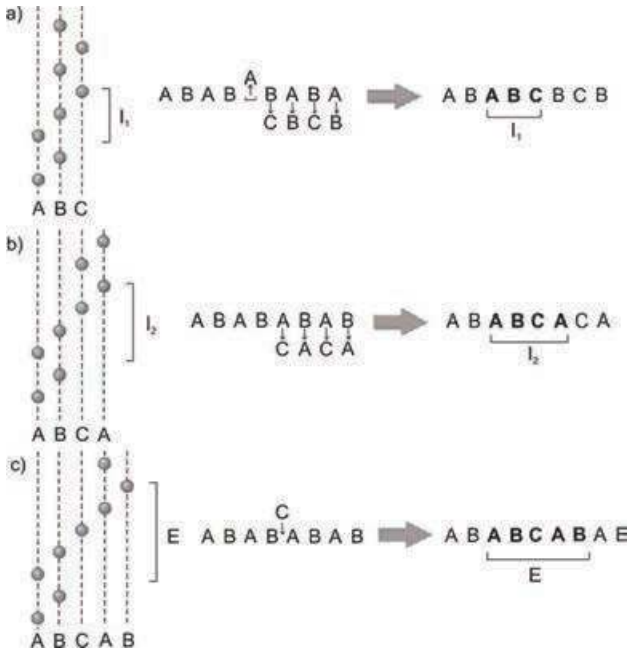

Figure 5.3: Stacking sequence of GaN with three types of BSFs. (a) Intrinsic BSF of type 1. (b) Intrinsic BSF of type 2. (c) Extrinsic BSF. Only atoms from one of the sublattices (Ga) are shown for clarity.

Besides BSFs, prismatic SFs (PSF), i.e. SFs on the planes perpendicular to c-plane, are also observed, for example faults on $(\bar{1}2\bar{1}0)$ plane with fault vector $\mathbf{R} = [10\bar{1}1]$. They were also found to terminate BSF [22]. The formation mechanism of SF is complex and poorly understood. It was proposed that SF are formed during growth process due to small difference in formation energies between wurtzite and cubic phases; another mechanism is impurity-induced SF formation [34]. SFs, in contrast to TDs, can be radiatively active. Zinc blende polytype of GaN has a lower bandgap energy of 3.2 eV compared to wurtzite structure with the bandgap energy of 3.4 eV at room temperature. Therefore, SF can be considered as a thin inclusion of cubic GaN and play a role of a QW where charge carriers can be confined. Excitons can be trapped by localization potential related to SF and recombine giving characteristic emission lines in the region 3.29-3.41 eV (Fig. 5 in **Paper 1**) [11]. It is agreed that these lines are related to SFs and partial dislocations terminating SFs, however there is still no clarity in the attribution of these peaks.

Chapter 6

Characterization Techniques

6.1 Transmission Electron Microscopy

TEM is a versatile microscopy technique that provides a wealth of information about morphology, composition, and crystallographic properties of the studied samples. The resolving power of a microscope is defined by the classical Rayleigh criterion and ultimately limited by the wavelength of radiation. Compared to photons, electrons have significantly smaller wavelength, therefore a much better resolution can be obtained if electrons are used instead of visible light, which is employed in TEM. The wavelength of electrons depends on their energy and defined by the following simple equation [35]:

$$\lambda = \frac{h}{\sqrt{2m_0eV}},$$

where h is Planck constant, m_0 is electron mass, V is potential drop.

If the energy of the electrons ($E = eV$) is equal to 200 keV, typical value in modern TEMs, then from this equation $\lambda \sim 2.7$ pm. Due to imperfect lenses, however, practical resolution is smaller, around 1 Å, which means that atomic size resolution is possible with TEM.

The typical design of a TEM is shown on Fig. 6.1. A highly energetic electron beam, generated by a field-effect emission gun, passes in a vacuum column through a series of condenser lenses and apertures that control beam's size and

intensity. Lenses are electromagnetic coils. The amount of electrical current flowing in the coil defines the strength of the lens. The beam interacts with a thin specimen, which is < 100 nm thick, part of the beam is transmitted and focused below the specimen by the objective lens, magnified by intermediate and projected by projection lenses onto the screen of a CCD camera.

A number of different imaging techniques and modes exist in TEM. Bright field (BF) imaging mode is the mode where only the transmitted beam is used to form the image: the central spot of diffraction pattern is chosen by introducing the objective aperture, filtering out most of the scattered electrons. Dark field (DF) mode, on the contrary, uses only the scattered electrons, by choosing spots other than the central one in the diffraction pattern. DF gives inverse and improved contrast relative to BF, which is advantageous for imaging smaller features in the crystal, such as extended defects. The contrast in BF and DF imaging is governed by diffraction phenomena.

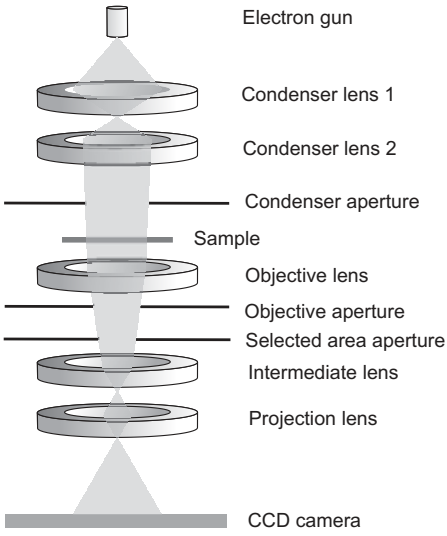

Figure 6.1: Schematic drawing of TEM.

At lower magnifications mass-thickness contrast prevails: thicker or denser areas appear darker, whereas thinner and lighter areas appear lighter. In high

resolution TEM (HRTEM) the contrast is produced by phase-contrast mechanism: when interacting with atom potentials electron wave undergoes phase shift, after the interaction, transmitted and scattered beams interfere to produce the contrast allowing for lattice resolution imaging.

Besides BF or DF images electron diffraction patterns give us information about the crystallography, orientation, and defects in the sample. The main drawback of TEM is the long and laborious sample preparation: cutting, grinding and ion milling are needed to make an electron transparent, less than 100 nm thin, TEM sample.

6.2 Scanning TEM and Energy-Dispersive X-ray Spectroscopy

Scanning TEM (STEM) is a TEM technique where instead of illuminating the sample with a parallel beam, a convergent beam is used to probe it. The electron rays are condensed by the lenses to a fine spot (< 1 nm) and scanned by means of scanning coils across the sample surface. Normally, high angle annular dark field (HAADF) detector is used to detect the signal. The contrast in this case is Z-contrast, i.e. intensity in the resulting image depends on the atomic scattering factor.

The power of TEM lies not only in the possibility for high magnification and for examining of the fine details, but also in extensive analytical capabilities available in the STEM mode. One of these techniques is Energy-Dispersive X-ray Spectroscopy (EDX). When the electron beam impinges onto the surface of the sample a great number of different signals is generated, among which X-rays are emitted. The energy of the X-rays is defined by the electronic structure of the constituent atoms in the material, therefore EDX scans give a picture of elemental composition in the sample. EDX is more suited for detecting heavier element atoms due to detector sensitivity limitations.

6.3 Scanning Electron Microscopy and Cathodoluminescence

Scanning electron microscopy (SEM) is another technique that harnesses electrons for imaging. Unlike TEM in SEM back-scattered or secondary electrons are detected to form the image. Similar to the case of STEM a probe, with a diameter of ~ 1 nm, made of an electron beam using several condenser lenses, is rastered with scanning coils across the sample surface. Much smaller accelerating voltages are applied to the electrons, in the range of 2 - 40 keV. Possible magnifications are from 10 to 500000 times. Samples with high dielectric constant, such as GaN on sapphire substrate, are glued to the sample holder with Ag paste or carbon films to avoid charging effects. SEM is widely used both in industry and academia as a tool for examination of microstructure and morphology of the films, since it is a non-destructive and quick characterization technique. Apart from the back-scattered and secondary electrons X-rays, Auger electrons and photons are generated during interaction of incoming electrons with the surface.

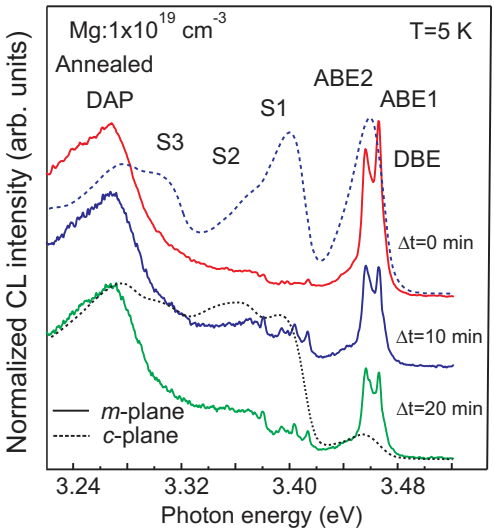

Figure 6.2: Typical CL spectra from c- and m-plane GaN.

Luminescence comes from the recombination of electrons that were excited to the conduction band from the valence band by the high-energy electron beam – this kind of luminescence is called cathodoluminescence (CL). A typical CL spectrum from *c*- and *m*-plane GaN samples studied in **Paper 1** and **Paper 2** are shown in Fig. 6.2. MonoCL4 system integrated with a LEO 1550 Gemini SEM used in our experiments is shown in Fig. 6.3. Either a fast CCD detection system or a Peltier cooled PMT were used for spectral acquisition. In CL the signal emanates from 1-8 μm depth of the sample depending on acceleration voltage. Direct comparison of structural features observed in SEM images with their optical properties obtained from CL spectra and CL mapping make the SEM-CL system a very powerful tool in characterization of semiconductors and ceramics.

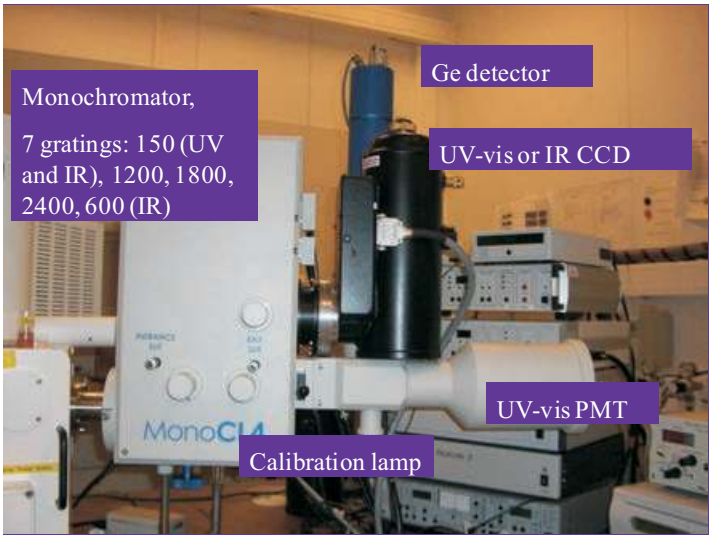

Figure 6.3: The MonoCL4 system at Linköping University.

Chapter 7

Summaries of the Papers

7.1 Paper 1

In **Paper 1** we have investigated the influence of Mg doping on optical and structural properties of *c*-plane GaN layers grown homoepitaxially by MOCVD. GaN films with varying Mg content (from 2×10^{18} cm^{-3} to 5×10^{19} cm^{-3}) were studied by TEM and low temperature CL. TEM investigations have shown that Mg incorporation in *c*-plane GaN results in SF formation. In particular, SFs of type I_1 and small characteristic length of $3 - 10$ nm have been found. Concentration of SFs increased with increasing Mg content. In contrast, no SFs have been detected in undoped GaN. CL spectra from moderate to high Mg-doped samples exhibit several SF-related peaks in the 3.3-3.41 eV range and show temporal metastability. The optical data suggest that the structural defects interact with the nearby Mg acceptors, and this interaction may be responsible for the observed metastability effects in CL spectra. The EDX line profile analysis performed across a SF has shown that the Mg-impurity atom can be found at a distance approximately 5 nm from the SF. CL mapping taken at the energies corresponding to SF-related peaks has confirmed that the corresponding CL came primarily from the Mg-doped regions of the samples.

7.2 Paper 2

In **Paper 2** Mg-doped *m*-plane GaN layers grown homoepitaxially by MOCVD have been studied using TEM and CL characterization techniques. TEM analysis of GaN:Mg layers have revealed the presence of BSFs with a rather high density ($\sim 10^6$ cm^{-1}) as well as several PSFs at the interface with the GaN substrate. However, the corresponding emissions in CL spectra (3.3-3.4 eV) were weak, instead a number of sharp lines at $\sim$ 3.4 eV was observed. Relation of these features to DAP recombination was excluded by calculations and experiments. By analogy with *p*-type GaAs case, these peaks may have excitonic character and be related to some low symmetry acceptor defect centers.

Bibliography

[1] F. A. Ponce and D. P. Bour. Nitride-based semiconductors for blue and green light-emitting devices. *Nature*, 386:351 – 359, 1997.

[2] H. Amano, N. Sawaki, I. Akasaki, and Y. Toyoda. Metalorganic vapor phase epitaxial growth of a high quality GaN film using an AlN buffer layer. *Applied Physics Letters*, 48(5):353, 1986.

[3] H. Amano, M. Kito, K. Hiramatsu, and I. Akasaki. P-Type Conduction in Mg-Doped GaN Treated with Low-Energy Electron Beam Irradiation (LEEBI). *Jpn. J. Appl. Phys.*, 28:L2112–L21148, 1989.

[4] S. Nakamura, T. Mukai, M. Senoh, and N. Iwasa. Thermal annealing effects on p-type Mg-doped GaN films. *Japanese Journal of Applied Physics*, 38:L139–L142, 1992.

[5] S. Nakamura, T. Mukai, and M. Senoh. Candela-class high-brightness InGaN/AlGaN double-heterostructure blue-light-emitting diodes. *Applied Physics Letters*, 64(13):1687, 1994.

[6] Q. Dai et al. Internal quantum efficiency and nonradiative recombination coefficient of GaInN/GaN multiple quantum wells with different dislocation densities. *Applied Physics Letters*, 94(11):111109, 2009.

[7] T. S. Ugahara, H. S. Ato, M. H. Ao, Y. N. Aoi, S. K. Urai, and S. T. Ottori. Direct Evidence that Dislocations are Non-Radiative Recombination Centers in GaN. *Japanese Journal of Applied Physics*, 37(4):398–400, 1998.

[8] N. G. Weimann, L. F. Eastman, D. Doppalapudi, H. M. Ng, and T. D. Moustakas. Scattering of electrons at threading dislocations in GaN. *Journal of Applied Physics*, 83(7):3656, 1998.

[9] J. H. You, J.-Q. Lu, and H. T. Johnson. Electron scattering due to threading edge dislocations in n-type wurtzite GaN. *Journal of Applied Physics*, 99(3):033706, 2006.

[10] C. F. Johnston, M. J. Kappers, M. a. Moram, J. L. Hollander, and C. J. Humphreys. Assessment of defect reduction methods for nonpolar a-plane GaN grown on r-plane sapphire. *Journal of Crystal Growth*, 311(12):3295–3299, 2009.

[11] R. Liu, A. Bell, F. A. Ponce, C. Q. Chen, J. W. Yang, and M. a. Khan. Luminescence from stacking faults in gallium nitride. *Applied Physics Letters*, 86(2):021908, 2005.

[12] H. Morkoç. *Handbook of Nitride Semiconductors and Devices*. Wiley-VCH, Berlin, 2008.

[13] V. S. Ban. Mass spectrometric and thermodynamic studies of the CVD of some iii-v compounds. *Journal of Crystal Growth*, 17:19–30, 1972.

[14] O. Ambacher, J. Smart, J. R. Shealy, N. G. Weimann, K. Chu, and M. Murphy. Two-dimensional electron gases induced by spontaneous and piezoelectric polarization charges in N- and Ga-face AlGaN / GaN heterostructures. *Journal of Applied Physics*, 85(6):3222–3233, 1999.

[15] B. Monemar and G. Pozina. Group III-nitride based hetero and quantum structures. *Progress in Quantum Electronics*, 24:239–290, 2000.

[16] P. Waltereit et al. Nitride semiconductors free of electrostatic fields for efficient white light-emitting diodes. *Nature*, 406(6798):865–8, 2000.

[17] K. Okamoto, H. Ohta, D. Nakagawa, M. Sonobe, J. Ichihara, and H. Takasu. Dislocation-Free m -Plane InGaN/GaN Light-Emitting Diodes on m -Plane GaN Single Crystals. *Japanese Journal of Applied Physics*, 45(45):L1197–L1199, Nov. 2006.

[18] D. F. Feezell et al. AlGaN-Cladding-Free Nonpolar InGaN/GaN Laser Diodes. *Japanese Journal of Applied Physics*, 46(4):L284–L286, Mar. 2007.

[19] B. Monemar. Bound excitons in GaN. *Journal of Physics: Condensed Matter*, 13:7011–7026, 2001.

[20] R. Ste. Symmetry of excitons in GaN. *Physical Review B*, 60(7):4438–4441, 1999.

[21] W. Liu, M. F. Li, S. J. Xu, K. Uchida, and K. Matsumoto. Phonon-assisted photoluminescence in wurtzite GaN epilayer. *Semiconductor Science and Technology*, (13):769772, 1998.

[22] D. Zakharov, Z. Liliental-Weber, B. Wagner, Z. Reitmeier, E. Preble, and R. Davis. Structural TEM study of nonpolar a-plane gallium nitride grown on $(11\bar{2}0)$4H-SiC by organometallic vapor phase epitaxy. *Physical Review B*, 71(23):1–9, Jun. 2005.

[23] S. K. Mathis, a. E. Romanov, L. F. Chen, G. E. Beltz, W. Pompe, and J. S. Speck. Modeling of Threading Dislocation Reduction in Growing GaN Layers. *Physica Status Solidi (a)*, 179(1):125–145, May 2000.

[24] A. Chakraborty et al. Demonstration of Nonpolar m -Plane InGaN/GaN Light-Emitting Diodes on Free-Standing m -Plane GaN Substrates. *Japanese Journal of Applied Physics*, 44(5):L173–L175, Jan. 2005.

[25] M. J. Kappers, M. a. Moram, D. V. Sridhara Rao, C. McAleese, and C. J. Humphreys. Low dislocation density GaN growth on high-temperature AlN buffer layers on (0001) sapphire. *Journal of Crystal Growth*, 312(3):363–367, Jan. 2010.

[26] X. H. Wu et al. Defect structure of metal-organic chemical vapor deposition-grown epitaxial (0001) GaN/Al_2O_3. *Journal of Applied Physics*, 80(6):3228, 1996.

[27] M. A. Moram and M. E. Vickers. X-ray diffraction of III-nitrides. *Reports on Progress in Physics*, 72(3):036502, Mar. 2009.

[28] X. J. Ning, F. R. Chien, and P. Pirouz. Growth defects in GaN films on sapphire: The probable origin of threading dislocations. *Journal of Materials Research*, 11(3), 1996.

[29] X. Wu et al. Dislocation generation in GaN heteroepitaxy. *Journal of Crystal Growth*, 189-190:231–243, Jun. 1998.

[30] V. Narayanan, K. Lorenz, W. Kim, and S. Mahajan. Origins of threading dislocations in GaN epitaxial layers grown on sapphire by metalorganic chemical vapor deposition. *Applied Physics Letters*, 78(11):1544, 2001.

[31] B. Beaumont and P. Venne. Epitaxial Lateral Overgrowth of GaN. *Physica Status Solidi (b)*, 43(1):1–43, 2001.

[32] M. a. Moram, M. J. Kappers, Y. Zhang, Z. H. Barber, and C. J. Humphreys. Very low dislocation density, resistive GaN films obtained using transition metal nitride interlayers. *Physica Status Solidi (a)*, 205(5):1064–1066, May 2008.

[33] D. Hull and D. J. Bacon. *Introduction to dislocations*. Elsevier.

[34] Z. Z. Bandic and T. C. Mcgill. Electronic structure of GaN stacking faults. *Physical Review B*, 56(7):3564–3566, 1997.

[35] D. B. Williams and C. B. Carter. *Transmission electron microscopy: a textbook for materials science*. Springer, 2009.